Electronic Supplementary Information

Smart magnetic nanopowder based on the manganite perovskite for local hyperthermia

A.V. Pashchenko,[abc] N.A. Liedienov,*[ab] I.V. Fesych,[d] Quanjun Li,[a] V.G. Pitsyuga,[e] V.A. Turchenko,[bf] V.G. Pogrebnyak,[c] Bingbing Liu[a] and G.G. Levchenko*[ab]

[a] State Key Laboratory of Superhard Materials, International Center of Future Science, Jilin University, 130012 Changchun, China
[b] Donetsk Institute for Physics and Engineering named after O. O. Galkin, NASU, 03028 Kyiv, Ukraine
[c] Ivano-Frankivsk National Technical University of Oil and Gas, MESU, 76019 Ivano-Frankivsk, Ukraine
[d] Taras Shevchenko National University of Kyiv, 01030 Kyiv, Ukraine
[e] Vasyl' Stus Donetsk National University, 21021 Vinnytsia, Ukraine
[f] Frank Laboratory of Neutron Physics, Joint Institute for Nuclear Research, 141980 Dubna, Russia

E-mail: nikita.ledenev.ssp@gmail.com (N.A. Liedienov), g-levch@ukr.net (G.G. Levchenko)

ESI1

Definition of coherent scattering size in the $La_{0.6}Ag_{0.2}Mn_{1.2}O_3$ nanopowder

The relationship between the broadening of the diffraction maximum and a decrease in the size of crystallites (coherent scattering regions) can be obtained from the Scherrer equation [1]:

$$D = K\lambda / \beta\cos\theta, \quad \text{(S1)}$$

where D is the scattering crystallites size in nm; $\lambda = 0.154178$ nm is the wavelength of the X-ray $Cu_{K\alpha}$-radiation; $K \approx 1$ is a Scherrer constant, which depends on the method for determining the line broadening and the crystal shape; β is the integral width of the reflex at half the maximum height in radians; and θ is the diffraction angle in degrees. The true integral width of the peak was calculated using the Warren formula [2]:

$$\beta = \sqrt{\beta_{\exp}^2 - \beta_0^2},$$

where β_{exp} is the experimental peak width at half the maximum intensity; and β_0 is the instrumental broadening of the diffraction line, which depends on the design features of the diffractometer. The resolution function of the diffractometer, β_0, was determined in another experiment from the diffraction pattern for the LaB_6 standard. For the $La_{0.6}Ag_{0.2}Mn_{1.2}O_3$ nanopowder, the average size of coherent scattering regions D_{012} = 62 ± 2 nm was obtained while approximating experimental values of the diffraction maximum (Bragg angle of $2\theta \approx 22.8°$) by the Lorentzian function (see figure S1) and taking into account all the experimental parameters in the Eq. (S1) (see Table S1).

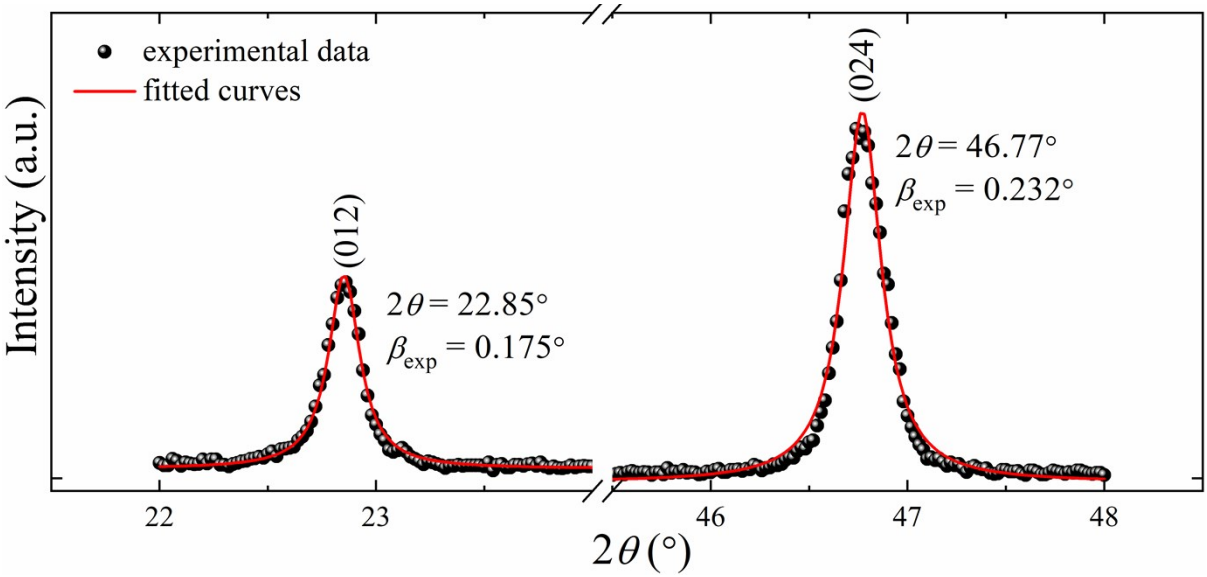

Figure S1. The diffraction pattern and its approximation by Lorentzian function for the $La_{0.6}Ag_{0.2}Mn_{1.2}O_3$ nanopowder in the region of the (012) and (024) reflections with the angles of $2\theta \approx 22.8°$ and $2\theta \approx 46.77°$.

Table S1

The experimental parameters of Scherrer equation (S1) for determining the average size of the coherent scattering regions D_{012} in the $La_{0.6}Ag_{0.2}Mn_{1.2}O_3$ nanopowder.

2θ (°)	β (radian)	cosθ	λ (nm)	K	D_{012} (nm)
22.85	0.0024	0.922	0.154187	1	62±2

The X-ray pattern (see figure S1) shows a single pair of non-overlapping lines with multiple Miller's indices (012) at $2\theta_I$ = 22.9° (peak I with the X-ray line half-width β_I) and

(024) at $2\theta_{II} = 46.8°$ (peak II with X-ray line half-width β_{II}). For a rhombohedral perovskite cell, the β_{II}/β_I ratio is in the range of $\cos\theta_I/\cos\theta_{II} < \beta_{II}/\beta_I < tg\theta_{II}/tg\theta_I$ [3]. An analysis of the coincidences $\beta_{II}/\beta_I \approx tg\theta_{II}/tg\theta_I$ or $\beta_{II}/\beta_I \approx \cos\theta_I/\cos\theta_{II}$ implies the reason for the broadening of the reflections. For $\beta_{II}/\beta_I \approx tg\theta_{II}/tg\theta_I$, the broadening of diffraction lines is determined by microstresses. For $\beta_{II}/\beta_I \approx \cos\theta_I/\cos\theta_{II}$, the broadening of diffraction lines is determined by a decrease in the crystallite size. If β_{II}/β_I is in the middle of this range, both these factors affect the broadening of diffraction lines. From Table S2, it can be seen that the β_{II}/β_I ratio is closer to the $\cos\theta_I/\cos\theta_{II}$ ratio. This indicates that in the region of small diffraction angles, the width of the X-ray lines is mainly determined by the size of the scattering crystallites, but not by microstresses. Therefore, the size of coherent scattering region was calculated using the Debye-Scherrer formula [1,2], but not the William-Hall method [4] which takes into account the effect of microstresses.

Table S2

The experimental angle parameters for the X-ray pattern (see figure S1) of the $La_{0.6}Ag_{0.2}Mn_{1.2}O_3$ nanopowder.

θ_I (°)	θ_{II} (°)	β_I (rad.)	β_{II} (rad.)	β_{II}/β_I	$\cos\theta_I/\cos\theta_{II}$	$tg\theta_{II}/tg\theta_I$
22.85	46.77	0.0024	0.0036	1.5	1.3	2.5

ESI2

Definition of the particle size distribution function in the magnetic $La_{0.6}Ag_{0.2}Mn_{1.2}O_3$ nanopowder

Analysis of the raster SEM images along the particle contour according to the scale factor makes it possible to plot the particle size distribution (see figure S2).

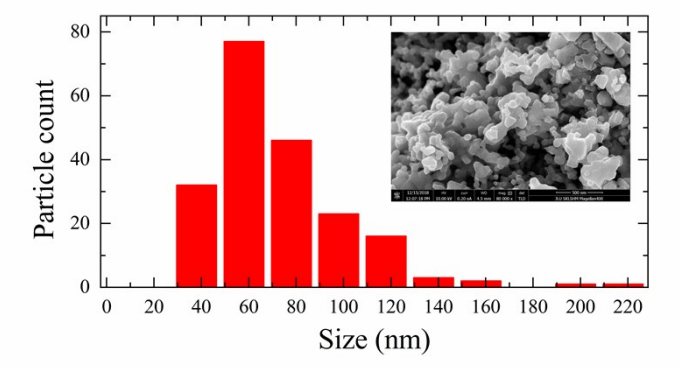

Figure S2. Particle size distribution according to SEM image (inset) for the $La_{0.6}Ag_{0.2}Mn_{1.2}O_3$.

While approximating particle size dispersion, three functions are usually used:

the Gaussian function $f(x) = A \cdot \exp\left[-\frac{(x-x_0)^2}{2\sigma^2}\right]$,

(S2)

the Lorentzian function $f(x) = \frac{2A}{\pi} \cdot \frac{\sigma}{4 \cdot (x-x_0)^2 + \sigma^2}$,

(S3)

the LogNormal Distribution function $f(x) = \frac{A}{\sqrt{2\pi}\sigma x} \cdot \exp\frac{-\left[\ln\frac{x}{x_0}\right]^2}{2\sigma^2}$,

(S4)

where A is a constant, x_0 is the mathematical expectation which corresponds to the average particle size, and σ^2 is the dispersion which means the size dispersion for the particle ensemble. The normalized $\int_0^{+\infty} f(x)dx = 1$ condition has been used to obtain the analytical form of $f(x)$ (see Table S3).

The best approximation of particle size dispersion was made by the LogNormal Distribution function (S4). The selection criterion was the highest approximation accuracy at which the determination coefficient R^2 takes the maximum value for the LogNormal Distribution (S4) (see figures S3 and S4, Table S3).

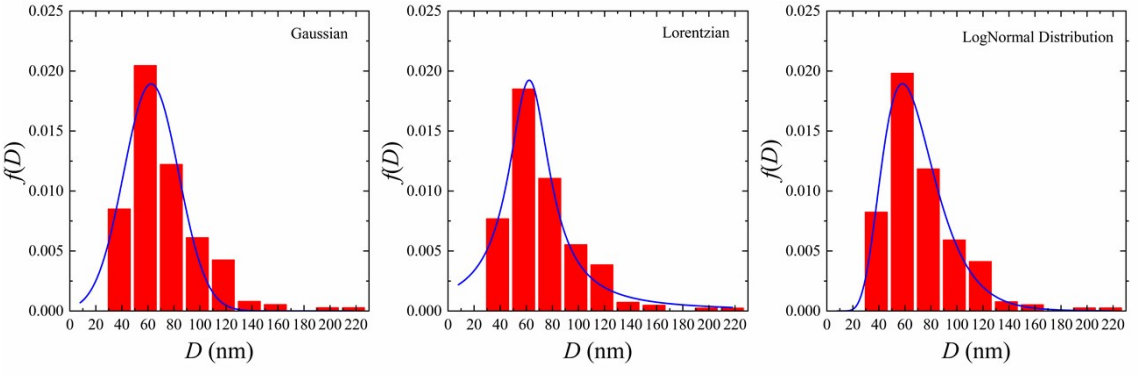

Figure S3. Approximation of the experimental values of the particle size D by the Gaussian function, the Lorentzian function, and the LogNormal Distributionfunction for the $La_{0.6}Ag_{0.2}Mn_{1.2}O_3$ nanopowder.

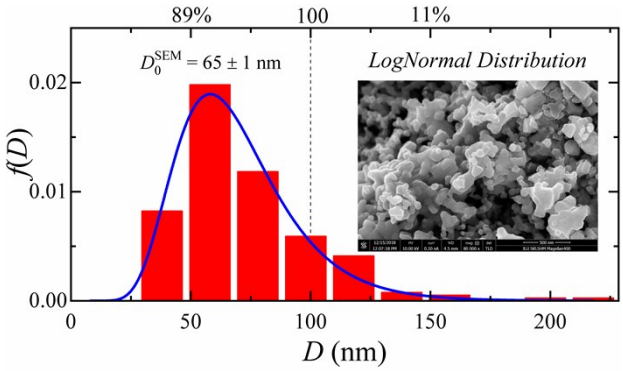

Figure S4. SEM image and the particle size distribution $f(D)$ (histogram) with its approximation (solid line) by the LogNormal Distribution as well as the average particle size D_0^{SEM} for the $La_{0.6}Ag_{0.2}Mn_{1.2}O_3$ nanopowder.

Table S3

The average particle size D_0, the particle size dispersion σ, the accuracy criteria χ^2 and R^2 at approximating the experimental values of the particle size by the Gaussian, the Lorentzian, and the LogNormal Distribution functions

Function	D_0, nm	σ, nm	χ^2	R^2
Gaussian	62.5±2.2	21.2±2.3	$3.3985 \cdot 10^{-6}$	0.93777
Lorentzian	62.3±1.5	38.9±4.1	$1.2668 \cdot 10^{-6}$	0.97166
LogNormal	65.3±1.2	24.4±1.5	$7.9539 \cdot 10^{-7}$	0.98448

The performed analysis made it possible to determine the average particle size D_0 = 65.3±1.2 nm in the $La_{0.6}Ag_{0.2}Mn_{1.2}O_3$ nanopowder and to establish that 89% of the particles had a size from 8 to 100 nm according to the condition $\int_0^{100} f(D)dD = 0.89$.

ESI3

The *A*- and *B*-structural positions, valence and magnetic states of manganese in non-stoichiometric $La_{0.6}Ag_{0.2}Mn_{1.2}O_3$ nanopowder

In the $La_{0.6}Ag_{0.2}Mn_{1.2}O_3$ material, manganese is the only magnetic ion, and the magnetic properties of the nanopowder depend on its valence and magnetic state. FM ordering appears as a result of a double exchange between the different valence ions Mn_B^{3+} and Mn_B^{4+}, which are in the *B*-positions of perovskite [5]. Superstoichiometric manganese Mn^{2+} occupies the *A*-positions and forms clusters [6] with AFM ordering at temperature T = 50 K (see figure 3) [7]. Therefore, the FM order at T_C is only associated with the ordering of Mn_B^{3+} and Mn_B^{4+}. In the PM region above T_C, all Mn_B^{3+}, Mn_B^{4+} and Mn_A^{2+}ions contribute to the total magnetic moment μ_{tot}(Mn) [8]:

$$\mu_{tot}(\mathrm{Mn}) = \sqrt{x_1 \cdot \mu^2_{\mathrm{Mn}^{2+}} + x_2 \cdot \mu^2_{\mathrm{Mn}^{3+}} + x_3 \cdot \mu^2_{\mathrm{Mn}^{4+}}}, \quad \text{(S5)}$$

where x_1, x_2 and x_3 are the concentrations of the Mn_A^{2+}, Mn_B^{3+}, and Mn_B^{4+} ions, respectively. The magnetic moments $Mn_B^{3+}(3d^4)$ with a spin S = 2 and $Mn_B^{4+}(3d^3)$ with a spin S = 3/2 equal $\mu_{\mathrm{Mn}^{3+}} = 4.90\mu_B$ and $\mu_{\mathrm{Mn}^{4+}} = 3.87\mu_B$, respectively [9]. Since $Mn_A^{2+}(3d^5)$ is in the cluster, its magnetic moment depends on the overlap of the electronic orbits between its nearest neighbours and may differ from the magnetic moment of a free ion. The appearance of clustered Mn_A^{2+} manganese can be represented as a disproportionate reaction [10],

$2\ Mn_B^{3+} = Mn_A^{2+} + Mn_B^{4+}$,

from which, the value of the magnetic moment $\mu_{Mn^{2+}} = 5.75\mu_B$ for clustered Mn_A^{2+} manganese is calculated. This agrees well with the experimental values 5.2–5.96μ_B for a free ion [11]. According to the electroneutrality principle, the molar formula of non-stoichiometric $La_{0.6}Ag_{0.2}Mn_{1.2}O_3$ composition can be written as $\{La^{3+}_{0.6}Ag^{1+}_{0.2}Mn^{2+}_{0.2}\}_A[Mn^{3+}_{0.4}Mn^{4+}_{0.6}]_BO^{2-}_3$ with concentrations $x_1 = 0.167$, $x_2 = 0.333$ and $x_3 = 0.5$. From Equation (S5), the total magnetic moment of manganese $\mu_{tot}(Mn) = 4.58\mu_B$ was calculated for the $La_{0.6}Ag_{0.2}Mn_{1.2}O_3$ nanopowder. It is in satisfactory agreement with the experimental value $\mu_{eff} = 4.61\mu_B$ obtained from the Curie–Weiss law (see figure 4). The coincidence of the calculated μ_{tot} and experimental μ_{eff} magnetic moments confirms the correctness of the structural position, valence, and magnetic states of manganese in the nanopowder of non-stoichiometric $La_{0.6}Ag_{0.2}Mn_{1.2}O_3$ composition.

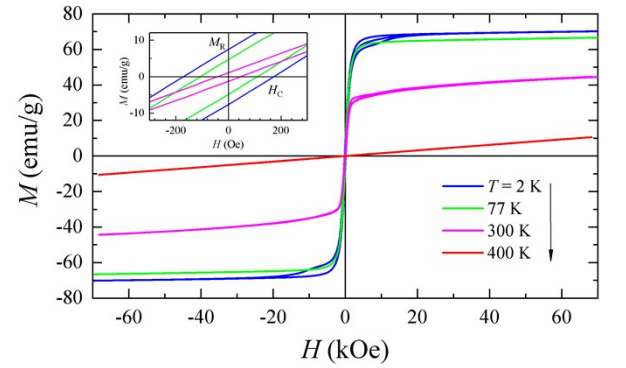

Figure S5. Hysteresis curves at $T = 2$, 77, 300, and 400 K.

Table S4

Saturation magnetization M_S, residual magnetization M_R, and coercivity H_C in the $La_{0.6}Ag_{0.2}Mn_{1.2}O_3$ nanopowder

T (K)	M_S		M_R		H_C (Oe)
	emu/g	emu/cm^3	emu/g	emu/cm^3	
2	69.7	426.8	7.5	46.6	172
77	65.9	403.4	4.9	30.4	109
300	34.1	208.8	1.1	6.8	51

ESI4

Calculation of the main magnetic characteristics of the $La_{0.6}Ag_{0.2}Mn_{1.2}O_3$ composition for local hyperthermia

Soft MNPs have two critical sizes: D_{cr}^{SD} is the size of the single-domain (SD) state, and D_{cr}^{MD} is the size of the multidomain (MD) state. With an increase in D, the transition from SD to MD occurs through a vortex state (VS) (see figure S6) [12].

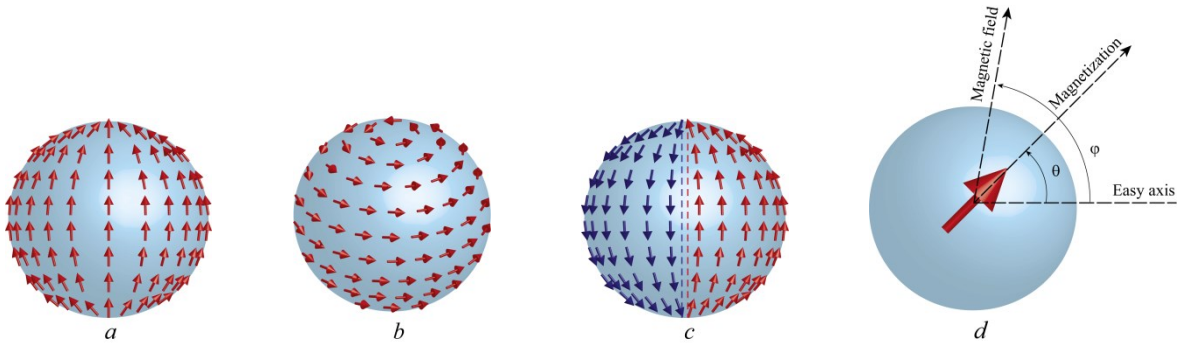

Figure S6. Spherical MNP with uniaxial magnetic anisotropy: uniform magnetization of the SD state (*a*); VS (*b*); MD state (*c*); the effect of magnetic field H on the magnetic moment M of a particle with uniaxial anisotropy (*d*).

The key role in the change in the magnetic state of the MNP is the energy balance between the exchange interaction energy E_{ex}, the magnetic anisotropy energy E_{ma} and the magnetostatic energy E_{ms} [13]. The exchange interaction E_{ex} establishes the magnetic order in materials. The magnetostatic energy E_{ms} is a magnetic energy of a particle in its own demagnetization field. To reduce the contribution of E_{ms} to the total energy, the FM material is divided into domains and goes into the MD state [14]. The magnetic anisotropy energy E_{ma} directs the magnetization vector along the easy axis. An exchange hardness A is the main quantitative parameter of the exchange interaction and equals [12]:

$$A = \frac{NJ_{ex}S^2}{a}, \qquad \text{(S6)}$$

where J_{ex} is the exchange integral; N is the number of magnetic ions in the unit cell; S is the spin quantum number; and a is the lattice constant. For a simple cubic lattice with $N = 1$, the exchange integral $J_{ex}$is related to the Curie temperature T_C as [15,16]:

$$J_{ex} = \frac{3k_B T_C}{ZS(S+1)}, \tag{S7}$$

where k_B is the Boltzmann constant; and Z is the number of nearest neighbours (for a simple cubic lattice $Z = 6$). The quantitative parameter of the magnetic anisotropy is the magnetocrystalline anisotropy constant K_1, which for hexagonal crystals with uniaxial magnetic anisotropy are related to the energy E_{ma} by the expression [12]:

$$E_{ma} = K_1 V \sin^2(\theta),$$

where K_1 is the uniaxial anisotropy constant, and θ is the angle between the magnetization and the direction of easy axis (see figure S6*d*).

The criterion for magnetic hardness is the parameter k. The parameter k shows how strong the contribution from the magnetic anisotropy energy E_{ma} is compared with the contribution from the magnetostatic energy E_{ms} [12]:

$$k = \frac{2K_1}{4\pi M_S^2}. \tag{S8}$$

In Brown's strict approach based on Kittel's estimation approach [17-19], the criteria of magnetic hardness for spherical MNPs with uniaxial anisotropy are determined as:

$k << 0.3562$ for soft magnetic particles, (S9)

$k \geq 0.3562$ for hard magnetic particles. (S10)

The exchange length l_{ex} is a characteristic length that shows how strong or weak the contribution from the exchange energy E_{ex} is compared with the contribution from the magnetostatic energy E_{ms} [13,20]:

$$l_{ex} = \sqrt{\frac{2A}{4\pi M_S^2}}. \quad \text{(S11)}$$

In the course of finding a balance between the energies of the particle in the SD and VS states, expressions for the critical sizes of the SD and MD states were obtained [13,17]:

$$D_{cr}^{SD} = 7.211\left(\frac{2A}{4\pi M_S^2}\right)^{1/2}, \quad \text{(S12)}$$

$$D_{cr}^{MD} = \frac{9.0584\cdot\left(\frac{2A}{4\pi M_S^2}\right)^{1/2}}{1-2.8075\cdot\frac{2K_1}{4\pi M_S^2}}. \quad \text{(S13)}$$

Substituting the $(2A/4\pi M_S^2)^{1/2}$ by l_{ex} from Equation (S11) and the hardness coefficient k from Equation (S8) into Equation (S12) and (S13), one can receive that the MNP can be in one of the three states depending on the size D:

$$D < D_{cr}^{SD} = 7.211\cdot l_{ex}, \text{ for SD state,} \quad \text{(S14)}$$

$$D_{cr}^{SD} < D < D_{cr}^{MD}, \text{ for VS state,} \quad \text{(S15)}$$

$$D > D_{cr}^{MD} = \frac{9.0584}{1-2.8075\cdot k}\cdot l_{ex}, \text{ for MD state.} \quad \text{(S16)}$$

Using Equations (S6), (S7), (S8), (S11), (7) for the $La_{0.6}Ag_{0.2}Mn_{1.2}O_3$ nanopowder with an average particle size D_0 = 65.3 nm, a Curie temperature T_C = 308 K, a saturation

magnetization M_S = 426.8 emu/cm^3 at T = 2 K, a blocking temperature T_B = 301 K, an effective anisotropy constant K_{eff} = 7.123·10^{3}erg/cm^3, and a magnetocrystalline anisotropy constant K_1 = 9.5·10^3 erg/cm^3, the main magnetic characteristics of the MNPs ensemble are determined.

References

[1] A.L. Patterson, The Scherrer formula for X-ray particle size determination. Phys. Rev. 56 (1939) 978. https://doi.org/10.1103/PhysRev.56.978

[2] B.E. Warren, X-ray diffraction methods. J. Appl. Phys. 12 (1941) 375. https://doi.org/10.1063/1.1712915

[3] S. S. Gorelik, L. N. Rastorguev, Yu. A. Skakov, X-Ray Diffraction and Electron Optical Analysis [in Russian], Metallurgiya, Moscow (1970).

[4] G.K. Williamson, W.H. Hall, X-ray line broadening from filed aluminium and wolfram. Acta Metall. 1 (1953) 22-31. https://doi.org/10.1016/0001-6160(53)90006-6

[5] J.M.D. Coey, M. Viret, S. Molnar, Mixed-valence manganites. Adv. Phys. 48 (1999) 167. https://doi.org/10.1080/000187399243455

[6] A.V. Pashchenko, V.P. Pashchenko, N.A. Liedienov, V.K. Prokopenko, Yu.F. Revenko, N.E. Pismenova, V.V. Burhovetskii, V.Y. Sycheva, A.V. Voznyak, G.G. Levchenko, V.P. Dyakonov, H. Szymczak, Structure, phase transitions, 55Mn NMR, magnetic and magnetotransport properties of the magnetoresistance La0.9−xAgxMn1.1O3−δ ceramics. J. Alloys Compd. 709 (2017) 779. https://doi.org/10.1016/j.jallcom.2017.03.093

[7] A.V. Pashchenko, V.P. Pashchenko, V.K. Prokopenko, Yu.F. Revenko, Yu.S. Prylipko, N.A. Ledenev, G.G. Levchenko, V.P. Dyakonov, H. Szymczak, Influence of structure defects

on functional properties of magnetoresistance (Nd0.7Sr0.3)1−xMn1+xO3 ceramics. Acta Materialia 70 (2014) 218. https://doi.org/10.1016/j.actamat.2014.02.014

[8] E. Zubov, A. Pashchenko, N. Nedelko, I. Radelytskiy, K. Dyakonov, A. Krzyżewski, A. Ślawska-Waniewska, V. Dyakonov, H. Szymczak,Magnetic and magnetocaloric properties of the La0.9−xAgxMn1.1O3 compounds. Low Temp. Phys. 43 (2017) 1190. https://doi.org/10.1063/1.5008411

[9] V. Dyakonov, A. Slawska-Waniewska, N. Nedelko, E. Zubov, V. Mikhaylov, K. Piotrowski, A. Szytula, S. Baran, W. Bazela, Z. Kravchenko, P. Aleshkevich, A. Pashchenko, K. Dyakonov, V. Varyukhin, H. Szymczak, Magnetic, resonance and transport properties of nanopowder of La0. 7Sr0. 3MnO3 manganites. J. Magn. Magn. Mater. 322(2010) 3072. https://doi.org/10.1016/j.jmmm.2010.05.032

[10] V.S. Zakhvalinskiĭ, R. Laiho, K.G. Lisunov, E. Lahderanta, P.A. Petrenko, Yu.P. Stepanov, J. Salminen, V.N. Stamov, Preparation and magnetic properties of LaMnO 3+ δ (0≤ δ≤ 0.154). Phys. Solid State 48 (2006) 2300. DOI: 10.1134/S1063783406120109

[11] S.V. Vonsovskii, Magnetism, (Nauka, Moscow), 1971, 1032 (Translated into English (J.Wiley, New York), 1974).

[12] P. Guimaraes, Nanoscience and technology (s.l. : Springer, Berlin, Heidelberg), 2009. 221.

[13] Yu.O. Tykhonenko-Polishchuk, A.I. Tovstolytkin, On the Critical Size of the Transition of a Ferromagnet into a Single-Domain State. J. Nano- Electron. Phys. 9 (2017) 02028. DOI: 10.21272/jnep.9(2).02028

[14] Yu.I. Gorobets, Yu.I. Dzhezherya, I.A. Melnichuk, S.V. Cherepov, A.P. Kuz', Application of domain structures elements of ferrite-garnet films for transport of magnetic microparticles. J. Appl. Phys. 108 (2010) 123902. https://doi.org/10.1063/1.3517111

[15] P.R.Weiss, The application of the Bethe-Peierls method to ferromagnetism. Phys. Rev. 74 (1948) 1493. https://doi.org/10.1103/PhysRev.74.1493

[16] S. Tikadzumi, Physics of Ferromagnetism. Magnetic Properties and Practice Applications. Translated into Russian under the title Fizika ferromagnetizma. Magnitnye kharakteristiki i prakticheskie primeneniya, (Moscow: Mir), 1987.

[17] W.F. Brown, The fundamental theorem of fine-ferromagnetic-particle theory. J. Appl. Phys. 39 (1968) 993. https://doi.org/10.1063/1.1656363

[18] C. Kittel, Theory of the structure of ferromagnetic domains in films and small particles. Phys. Rev. 70 (1946) 965. https://doi.org/10.1103/PhysRev.70.965

[19] C. Kittel, Physical theory of ferromagnetic domains. Rev. Mod. Phys. 21 (1949) 541. https://doi.org/10.1103/RevModPhys.21.541

[20] G.S. Abo, Y.-Ki. Hong, J. Park, J. Lee, W. Lee, B.-Ch. Choi, Definition of magnetic exchange length. IEEE Trans. Magn. 49 (2013) 4937. DOI: 10.1109/TMAG.2013.2258028